Planning of Gamma Knife Radiosurgery (GKR) for brain arteriovenous malformations using triple Magnetic Resonance Angiography (triple-MRA).

Alvaro Rojas-Villabona[1,2], Magdalena Sokolska[3], Thomas Solbach[4], Joan Grieve[5], Marilena Rega[6], Francisco Torrealdea[7], Francesca Benedetta Pizzini[8], Enrico De Vita[9], Yuriko Suzuki[10], Matthias JP Van Osch[10], Emma Biondetti[11], Karin Shmueli[11], David Atkinson[7], Mary Murphy[5], Ian Paddick[1], Xavier Golay[12], Neil Kitchen[5], Hans Rolf Jäger [4,12]

[1] *The Gamma Knife Centre at Queen Square, National Hospital for Neurology and Neurosurgery, London, UK*

[2] *Department of Neurosurgery, Royal Victoria Infirmary, Newcastle upon Tyne, UK*

[3] *Medical Physics and Biomedical Engineering, University College London Hospitals, London, UK*

[4] *The Lysholm Department of Neuroradiology, National Hospital for Neurology and Neurosurgery, London, UK*

[5] *Department of Neurosurgery, National Hospital for Neurology and Neurosurgery, London, UK*

[6] *Institute of Nuclear Medicine, University College London Hospitals, London, UK*

[7] *Centre for Medical Imaging, University College London, London, UK*

[8] *Radiology, Department. of Diagnostic and Public Health, Verona University, Verona, Italy*

[9] *Department of Biomedical Engineering, King's College London, London, UK*

[10] *C. J. Gorter Center for High Field MRI, Department of Radiology, Leiden University Medical Center, Leiden, Netherlands*

[11] *MRI Group, Department of Medical Physics and Biomedical Engineering, University College London, London, UK*

[12] *Academic Neuroradiological Unit, Department of Brain Repair and Rehabilitation, Institute of Neurology, University College London, London, UK*

Correspondence:

Alvaro Rojas-Villabona, Department of Neurosurgery, Royal Victoria Infirmary, Queen Victoria Road, Newcastle upon Tyne, UK. NE1 4LP; Tel: 0191 233 6161; email: a.villabona.11@ucl.ac.uk

Running head: Triple-MRA for planning of Gamma Knife Radiosurgery for AVMs

Word count: 4039

Authors' contributions: All authors made a significant contribution to the study.

Previous presentations: This manuscript has not been previously published in whole or in part. Portions of this work were presented in abstract form at the meeting of the International Leksell Gamma Knife Society meeting in Dubai, UAE, (oral presentation, 07 March 2018) and the 25th meeting of the International Society for Magnetic Resonance in Medicine, Honolulu, Hawaii, USA (e-poster presentation, 26 April 2017).

Funding: This project was supported by The National Brain Appeal (Small Acorns grant awarded to Alvaro Rojas-Villabona), Queen Square Radiosurgery Centre, Elekta (UK) Limited and the Engineering and Physical Sciences Research Council (EPSRC - First grant EP/K027476/1 awarded to Karin Shmueli). Brainlab AG provided the Elements software free of charge for triple-MRA post-processing. The study was also sponsored by the BRC.

Abstract

Purpose: Intra-arterial Digital Subtraction Angiography (DSA) is the gold standard technique for radiosurgery target delineation in brain Arterio-Venous Malformations (AVMs). This study aims to evaluate whether a combination of three Magnetic Resonance Angiography sequences (triple-MRA) could be used for delineation of brain AVMs for Gamma Knife Radiosurgery (GKR).

Methods: Fifteen patients undergoing DSA for GKR targeting of brain AVMs also underwent triple-MRA: 4D Arterial Spin Labelling based angiography (ASL-MRA), Contrast-Enhanced Time-Resolved MRA (CE-MRA) and High Definition post-contrast Time-Of-Flight angiography (HD-TOF). The arterial phase of the AVM nidus was delineated on triple-MRA by an interventional neuroradiologist and a consultant neurosurgeon (triple-MRA volume). Triple-MRA volumes were compared to AVM targets delineated by the clinical team for delivery of GKR using the current planning paradigm, i.e. stereotactic DSA and volumetric MRI (DSA volume). Difference in size, degree of inclusion (DI) and concordance index (CcI) between DSA and triple-MRA volumes are reported.

Results: AVM target volumes delineated on triple-MRA were on average 9.8% smaller than DSA volumes (95%CI:5.6-13.9%; SD:7.14%; p=0.003). DI of DSA volume in triple-MRA volume was on average 73.5% (95%CI:71.2-76; range: 65-80%). The mean percentage of triple-MRA volume not included on DSA volume was 18% (95%CI:14.7-21.3; range: 7-30%).

Conclusion: The technical feasibility of using triple-MRA for visualisation and delineation of brain AVMs for GKR planning has been demonstrated. Tighter and more precise delineation of AVM target volumes could be achieved by using triple-MRA for radiosurgery targeting. However, further research is required to ascertain the impact this may have in obliteration rates and side effects.

Key words: Arteriovenous Malformations, Magnetic Resonance Angiography, Gamma Knife Stereotactic Radiosurgery, Cerebral Angiography, Treatment Planning.

Introduction

Gamma Knife Radiosurgery (GKR) of brain Arterio-Venous Malformations (AVM) is aimed at eliminating the risk of intracranial haemorrhage by obliterating the nidus and shunt of the AVM, with minimal injury to surrounding normal brain tissue (van Beijnum et al., 2011). This is achieved by stereotactically delivering a high and greatly localized radiation dose to the AVM nidus (Leksell, 1983, Seymour et al., 2016). It is well accepted that higher obliteration rates and less complications are achieved when inclusion of the entire AVM nidus in the treatment volume is accomplished while excluding draining veins and neovascularisation (Safain et al., 2014). Intra-arterial Digital Subtraction Angiography (DSA), alongside volumetric MR and/or CT imaging, has historically been the main imaging modality used for radiosurgery target delineation in AVM radiosurgery, and it is still considered the gold standard technique (Pollock et al., 2017, Starke et al., 2017). However, DSA data usually integrated into the GKR planning system consists of two-dimensional (2D) projections and does not contain 3D information (Taschner et al., 2007). DSA also has a small but definite risk of neurological complications related to thromboembolic events. This lies between 0.3% and 2.6% per examination and increases when multiple DSA procedures are performed, often the case in the AVM population (Fifi et al., 2009, Kaufmann et al., 2007, Dawkins et al., 2007, Leffers and Wagner, 2000). Silent embolic events are also found on diffusion weighted MRI in up to 23% of the patients after DSA (Bendszus et al., 1999) and severe complications such as stroke with permanent disability (0.14%) and death (0.06%) have been reported (Kaufmann et al., 2007). DSA also exposes both patients and medical staff to ionizing radiation, it carries the risk associated with injection of iodinated contrast agents and it is an unpleasant experience for patients due to pain, invasiveness and prolonged bed rest after the procedure (Fifi et al., 2009). Targeting of AVMs using non-invasive imaging is a desirable, but yet to be accomplished, improvement to the GKR planning procedure.

Several studies have previously attempted to use alternative techniques for AVM radiosurgery targeting including Time-Of-Flight angiography (TOF), CT angiography and 4D imaging such as time resolved Contrast-Enhanced MR angiography (CE-MRA), with varying degrees of success (Nagaraja et al., 2005, Bednarz et al., 2000, Taschner et al., 2007, Kang et al., 2014, St George et al., 2002, Hamm et al., 2008, Amponsah et al., 2012, Buis et al., 2007). However, none of those angiography techniques has been shown to individually enable accurate

delineation of AVMs and produce radiosurgical targets comparable to those obtained with DSA in terms of size and conformity. This study aims to evaluate whether a combination of High Definition post-contrast TOF angiography (HD-TOF), time-resolved CE-MRA and 4D Arterial Spin Labelling based angiography (ASL-MRA), referred to as triple-MRA, could be used for visualisation and delineation of brain AVMs for GKR targeting.

Methods

Patients

Fifteen consecutive adult patients undergoing GKR for brain AVMs at the Gamma Knife Centre at Queen Square between June 2015 and October 2016 were prospectively recruited. The research pathway and image analysis framework used for AVM target delineation with DSA and triple-MRA, are shown in the flow diagram in figure 1.

All participants gave written consent for a triple-MRA to be performed before GKR and the study was approved by the Queen Square research ethics committee (IRB). Exclusion criteria: Inability to undergo MR imaging without sedation/anaesthesia, impaired renal function (eGFR < 30ml/min), inability to consent, pregnancy, allergy to gadolinium, contraindication to MRI (i.e., pacemakers) and history of coiling of cerebral aneurysms.

Triple-MRA imaging protocol

Triple-MRA included non-stereotactic (without a stereotactic frame) ASL-MRA, CE-MRA and post-contrast HD-TOF acquired with the parameters shown in table 1. The selection of a high spatial definition MRA sequence (HD-TOF) and two time resolved (4D) MRA sequences (ASL-MRA and CE-MRA) was done to maximise temporal and spatial resolution which have been identified as limiting factors in previous studies that used individual MRA sequences for AVM targeting (Nagaraja et al., 2005, Bednarz et al., 2000, Taschner et al., 2007, Kang et al., 2014, St George et al., 2002, Hamm et al., 2008, Amponsah et al., 2012, Buis et al., 2007).

Triple-MRA was acquired using a 32-channel Achieva® 3.0 T MRI system (Philips Healthcare Systems, Best, The Netherlands). The median time between triple-MRA and GKR was 10 days (range, 2–87 days); it was more than 30 days in four patients.

A fast ASL-MRA survey with Echo Planar Imaging (EPI) and Turbo Field Echo (TFE) acceleration was used to characterise the filling velocity of the AVM in each individual case as shown in figure 2. The ASL survey encompassed 8 dynamic phases with a temporal resolution of 200 ms (Suzuki et al., 2018). A 300 mm Signal Targeting with Alternating Radiofrequency (STAR) labelling slab was positioned below the imaging plane and a small (10mm) axial slab including part of the AVM nidus was scanned in 54 seconds (table 1). The three time points that best showed the arterial phase of the AVM nidus were then acquired with the substantial ASL-MRA sequence which had better spatial resolution and pulsation artefact robustness (non-EPI). There was a significant degree of variability between patients in terms of optimal label delay which ranged from 200-800 ms (mean: 470 ms; SD: 212 ms) and phase interval -time between dynamic frames- which ranged from 200 to 300 ms (mean: 236 ms). For this reason, ASL-MRA scanning time varied among patients from 5:58 to 12:24 min (mean: 8:46 min).

CE-MRA was acquired using a 3D, T1 weighted, Fast-Field Echo (FFE) sequence and it included 24 dynamic time points. A manual IV bolus injection of 0.2 mL/kg of Gadobenic acid 0.5 M (MultiHance®, Milan, Italy) was performed over an estimated time of 4 seconds followed by a saline flush of 20 ml. The fast dynamic acquisition was started at the same time as the injection, it had a temporal resolution of 608 ms/phase and used contrast-enhanced robust-timing angiography (CENTRA) and the keyhole method with 20% of the k-space collected per keyhole frame (Willinek et al., 2008). HD-TOF acquisition started approximately 10 minutes after injection of gadolinium. It was based on a 3D-FFE acquisition with flow compensation and tilt-optimized non-saturated excitation (TONE) across the slab (Wrede et al., 2014). Four slabs covering 50 mm in the cranio-caudal direction were obtained with parallel imaging, SENSE factor of 2.

DSA protocol and stereotactic MRI for GKR planning

The stereotactic method used at Queen Square has been described elsewhere (Rojas-Villabona et al., 2016). Stereotactic DSA was performed using a biplane system (Artis zee Biplane, Siemens, Erlangen, Germany) and iodinated contrast agent (Iohexol 240 mg/ml, Omnipaque,

GE Healthcare, Cork, Ireland). A femoral artery approach was used for selective contrast injection of one or several vessels. DSA was performed at a rate of 3-7 frames/second in standard orthogonal planes for a time resolution of 133 - 333 ms. The DSA spatial resolution was 0.3 mm (1024 x 1024 matrix). For GKR planning a review of the DSA series by the interventional neuro-radiologist was performed to select one or a few time points in the early arterial phase. These were then imported into Leksell GammaPlan 10.1 (Elekta Instrument AB, Stockholm, Sweden) and defined into the stereotactic coordinates system, together with stereotactic 3D T1 and T2 weighted MRI for targeting.

Imaging used for delineation of a DSA based volume included: stereotactic DSA, stereotactic T2 weighted and post-contrast T1 weighted MRI and HD-TOF (figure 3). For this, the early arterial phase of the AVM nidus was delineated on 2D DSA in consensus by the practising consultant neurosurgeon and interventional neuroradiologist who performed the DSA procedure using Leksell GammaPlan 10.1. The limits of the AVM ROI delineated on 2D DSA images were then projected into volumetric MRI defining an area within which the AVM is contained. The 3D volume was then drawn within this area on volumetric scans. The resultant volume (DSA volume) was used to develop a radiosurgery treatment plan that was delivered to the patients with the Leksell Gamma Knife Perfexion (Elekta Instrument AB).

AVM target definition on triple-MRA

ASL-MRA, CE-MRA and HD-TOF data were transferred to the Brainlab Elements platform (Brainlab AG, Munich, Germany) for post-processing. The volumetric datasets of all three ASL-MRA time points and selected CE-MRA time points were individually co-registered with HD-TOF using Brainlab Merge Element which uses multimodal rigid image registration with cranial distortion correction and has a co-registration accuracy of < 1 mm within the intracranial cavity (Brainlab, 2017, Brainlab, 2011). The quality of co-registration was validated using intracranial arteries as landmarks, namely, middle cerebral artery bilaterally, the pericallosal and marginal arteries superiorly and the basilar artery bifurcation inferiorly. The overlap of these blood vessels in the co-registration pairs was visually assessed in all three orthogonal planes and ROIs were defined to improve the quality of co-registration where necessary. Maximum Intensity Projections (MIPs) with 360 degrees of rotation were generated for all MRA sequences (figure 3).

Triple-MRA based volumes were delineated using the semi-automatic drawing tool SmartBrush Element (Brainlab AG) by including areas shown to be part of the AVM nidus on ASL-MRA, CE-MRA and HD-TOF excluding draining veins. This was done in consensus by a team comprised of an interventional neuroradiologist and a consultant neurosurgeon (TS and JG), both with more than 15 years of experience. They had not been involved with the treatment planning of the study subjects and were blinded to DSA volumes.

Data analysis

The percentage difference between DSA and triple-MRA volumes was calculated and further analysed using one-sample t-test and the Bland–Altman plot. Statistical analyses were performed using the Statistical Package for the Social Sciences (SPSS Statistics, Version 23. IBM Corp) and statistical significance was defined as a *p* value of <0.05. Comparison of volumes in terms of inclusion and concordance was performed off-line using MATLAB 9.2 (The MathWorks Inc, Natick, Massachusetts, USA). Degree of inclusion (DI) is the percentage of DSA volume (DSAv) included in triple-MRA volume (tMRAv) calculated using equation 1, where ∩ is the intersection between two volumes:

$$\mathrm{DI\ (DSAv\ in\ tMRAv)} = \left(\frac{\mathrm{DSAv} \cap \mathrm{tMRAv}}{\mathrm{DSAv}}\right) \times 100 \ [1]$$

The percentage of triple-MRA volume not included in DSA volume, termed degree of non-inclusion (DnI), is given by equation 2:

$$\mathrm{DnI\ (tMRAv\ not\ in\ DSAv)} = \left(1 - \frac{\mathrm{DSAv} \cap \mathrm{tMRAv}}{\mathrm{tMRAv}}\right) \times 100 \ [2]$$

The Concordance Index (CcI) of DSA and triple-MRA volumes is the ratio of the intersection to the union (∪) of the two volumes (equation 3), as described by Jaccard (Jaccard, 1912). The maximum CcI value is 1 if the two volumes are identical, and the minimum is 0.

$$\mathrm{CcI} = \frac{\mathrm{DSAv} \cap \mathrm{tMRAv}}{\mathrm{DSAv} \cup \mathrm{tMRAv}} \ [3]$$

Results

Participants

Table 2 shows the demographic details and AVM characteristics of the study subjects. Mean age was 38 years (range: 18-62) and 10 patients (66%) were female. The lesions were Spetzler-Martin grade 1 and 2 in 43% of the cases, grade 3 in 42% of the patients and high-grade AVMs (4 and 5) were observed in 15% of them. Three subjects had undergone partial glue embolization before GKR, one of them on two occasions, and none of them had previously undergone surgical excision. One patient declined GKR after triple-MRA and they were excluded from the final statistical analysis which included 14 subjects. Total triple-MRA scanning time ranged from 19:05 to 25:33 min (mean: 21:53 min). It varied among patients due to individualised timing of ASL-MRA.

Triple-MRA vs DSA target volumes

AVM target volumes obtained using the standard DSA method and triple-MRA are presented in table 3. The mean DSA volume, drawn by the neurosurgical team for delivery of GKR using 2D projections of DSA and volumetric MRI, was 3.89 ml (95%CI: 1.95-5.82 ml; SD: 3.35 ml; median: 3.35 ml; range: 0.1-10.77 ml). AVM volumes delineated on triple-MRA were on average 9.8% smaller than DSA volumes (95%CI: 5.6-13.9%; SD:7.14%; p=0.003). The mean triple-MRA volume was 3.49 ml (95%CI: 1.77 – 5.2 ml; SD: 2.97 ml; median: 2.88 ml; range: 0.09-9.89 ml) and was smaller than the DSA volume in all but one case (figure 4).

DI of DSA volume in triple-MRA volume was on average 73.5% (95%CI: 71.2-76%; SD: 4.1%; median: 73%; range: 65-80%). It was above 70% in all subjects except for case 9, in which a small difference between the volumes represented a high percentage discrepancy due to the very small size of the target (0.103 ml, figure 5). The mean percentage of triple-MRA volume not included on DSA (DnI) was 18% (95%CI: 14.7-21.3%; SD: 5.7%; median: 18.4%; range: 7-30%). It was 20% or less in all subjects except for two cases. One of these was case 9 (30%) for the same reason stated above (figure 5). The other case (26%) was the only subject in which triple-MRA volume (2.27 ml) was larger than DSA volume (2.10 ml). This was due to the inclusion on triple-MRA volume of an area in the medial aspect of the AVM nidus which appeared abnormal on triple-MRA, T1 post-gad and T2 but only slight

and diffuse vasculature was seen on DSA (case 10, figure 6).

The mean CcI was 0.63 (95%CI: 60.4-66.2; SD: 0.05; median: 0.63; range: 0.51-0.72). CcI was above 0.6 in all other cases but one in which the discrepancies described above also had a considerable effect on CcI (0.52, case 9). There was a weak correlation between CcI and AVM volume (Spearman's rank correlation coefficient, rho=0.54; p=0.047) driven mainly by case 9 which had the smallest volume and lowest CcI in the group. This correlation was not seen if case 9 was excluded (rho=0.42; p=0.15). No correlation was observed between CcI and age (p=0.83) or Spetzler-Martin grade (p=0.89). There was no difference on CcI between groups of gender (p=0.45), previous bleeds (p=0.45) or treatments (p=0.09), laterality (p=0.7), AVM location (p=0.18), surrounding brain eloquence (p=0.36), venous drainage pattern (p=0.75) and AVM density assessed on DSA as diffuse vs compact (p=0.5; Mann–Whitney U test).

Imaging quality

The AVM nidus was clearly identified on all three MRA techniques in all but 2 cases. In one case, the lesion was not seen on ASL-MRA due to the very superficial location in the posterior fossa, with the ASL labelled blood losing its tagging before reaching the AVM (case 12). In the other case, shown in figure 2, it was not possible to visualize the AVM in CE-MRA because the acquisition did not include the arrival of gadolinium bolus due to accidental mistiming of the injection with respect to the dynamic acquisition. However, in both cases the lesions were well depicted by the other two MRA sequences and their results in terms of CcI were no different to the rest of the cases (p=0.1).

Discussion

This study aimed to evaluate whether the combination of three MRA modalities could be used for delineation of brain AVMs for GKR targeting. In a group of patients undergoing GKR, the AVM nidus was delineated on triple-MRA and compared to the AVM target defined for GKR treatment using the current planning paradigm (DSA volume). The use of DSA for AVM radiosurgery planning could have been abandoned, without reservations, if no difference whatsoever was detected between triple-MRA and DSA volumes. That was, however, not the outcome of the study. Triple-MRA volumes were on average 9.8% smaller than DSA volumes. This was a statistically significant difference and only in one case was triple-MRA volume larger than DSA volume (figure 6).

Difference between triple-MRA and DSA volumes

It is not difficult to envisage that complex and irregular objects such as AVMs can be delineated in a more refined manner on volumetric and time resolved (4D) imaging such as triple-MRA. That is likely to be the reason for our finding of smaller AVM volumes with triple-MRA compared to the traditional planning method based on DSA. DSA provides only 2-dimensional projections of the AVM nidus and spatial information is lost because of dimensional reduction (Colombo et al., 2003). Volumes rendered from data with reduced dimensions are likely to be overestimated due to superimposition of feeding arteries and draining veins and difficulties in determining complex 3D irregularities on nidus geometry (Huang et al., 2017). The major accomplishment of triple-MRA is the combination of temporal and spatial resolution, which are necessary to appreciate the dynamic characteristics of intracranial vasculature and lesions such as AVMs. Additionally, dynamic information provided by triple-MRA can improve target delineation by better differentiation of AVM components; in particularly, identification of AV shunting and distinction between nidus and draining veins.

It is not possible to tell from our study if the 9.8% reduction in target size accomplished by triple-MRA delineation would impact clinical outcomes, in particular obliteration rates. This is because triple-MRA volume in our study was obtained for comparison purposes only and GKR was delivered to the patients using the DSA volume. The relatively similar response rate reported by multiple GKR centres with different target delineation methods and levels of expertise suggests that small differences in target size are unlikely to impact obliteration rates

(Kano et al., 2012, Koltz et al., 2013, Starke et al., 2017). Before CT and MRI were introduced, treatment planning for AVMs was based on DSA only and 3D delineation of radiosurgical targets was not used at all (Lunsford et al., 1991, Kemeny et al., 1989). Still, their reported two-years obliteration rates of 70-80% were not different from modern GKR outcomes. Also, the improvement of GKR planning methods that has taken place over the last few decades with development of planning software, did not increase obliteration rates either. Recent reports of patients treated with GKR using MRI only (without DSA) have showed no difference in obliteration rate (Amponsah et al., 2012) and contemporary groups that do not delineate a radiosurgical target on their planning imaging also achieve similar results in terms of obliteration (Levrier et al., 2001). Differences in Adverse Radiation Effects (ARE) have certainly been noted between groups, but response rates do not appear to significantly differ, which suggests that a 9.8% reduction in volume target is unlikely to compromise response rate. There is extensive evidence demonstrating that larger AVM target volumes result in higher rates of both symptomatic and radiological ARE (Cohen-Inbar et al., 2015, Kano et al., 2017, Yen et al., 2013). Therefore, if anything AVM radiosurgery targeting using triple-MRA volumes should result in lower ARE rates. However, these statements cannot be inferred nor concluded from our study and further research is warranted to explore these issues.

The differences between DSA and triple-MRA volumes in our study were not limited to size, though. There was also a degree of discrepancy in terms of conformity which was quantified using DI (73.5%; range: 65-80%), DnI (18%; range: 7-30%) and CcI (0.63; range: 0.51-0.72). The fact that triple-MRA volumes are smaller than DSA volumes directly affects these parameters, however inter-observer variability must have also caused part of this discrepancy. In our study triple-MRA and DSA volumes were delineated by two different teams to avoid recall bias and it is not possible to quantify the degree of uncertainty that this could have added to the results. Inter-observer variability is a well-recognised issue in AVM radiosurgery and it has been well quantified elsewhere (Al-Shahi et al., 2002, Buis et al., 2005, Sandström, 2011). Buis et al evaluated the extent of inter-observer variation in DSA contours of 31 AVMs by six independent GKR practitioners. The reported ratio between the volumes of agreement and the corresponding encompassing volumes (CcI) for all possible pairs of observers was 0.45 ± 0.18. It dropped to 0.19 ± 0.14 when calculated for all six volumes together (Buis et al., 2005). In our study, concordance was considerably better and even in our worst case CcI was not as poor as their average estimate. Sandström et al also

studied inter-observer variability of AVM delineation for GKR and reported a mean CcI of 0.63 (range: 0.24 to 0.81) for all pairs of observations which is strikingly similar to the CcI we found between DSA and triple-MRA volumes. The estimates of inter-observer variability reported by these studies are based on AVM target volumes delineated by active radiosurgery practitioners and they reflect a degree of uncertainty that is already incorporated and accepted in standard GKR practice.

Study limitations

Tighter and more precise delineation of AVM target volumes without the use of DSA is a desirable improvement for GKR and our study provides promising results on the technical feasibility of using multi-modality MRA for GKR planning as well as the quality of currently available MRA sequences. However, our study was limited by a small sample size. This was determined by the available resources, and the role of triple-MRA for planning of GKR for AVMs will need to be studied in a larger number of subjects before it can be used as a sole modality for GKR planning. The analysis of a larger number of subjects will help identify subgroups of patients, or AVM features, with extremes of concordance between DSA and triple-MRA volumes. This can help direct case selection and individualised imaging for planning. For instance, previous embolization has been repeatedly described as a confounder on AVM target delineation, but our group included only three patients with history of embolization. More data is required to make conclusions in this regard. In our study, we did not identify any variable affecting the quality of target delineation on triple-MRA but it has been previously suggested that selected AVM cases could be adequately targeted without a DSA (Taschner et al., 2007, Yu et al., 2004, Buis et al., 2007). Yu et al assessed the feasibility of AVM delineation on MRI only for GKR and concluded that it was adequate for cases with non-diffuse and large non-embolised AVMs (Yu et al., 2004). Buis et al concluded that TOF angiography might be used as the sole imaging modality for radiosurgical treatment of AVMs smaller than 3 ml if they were located in non-eloquent areas (Buis et al., 2007). Most GKR practitioners probably also remember cases of small, compact and non-eloquent AVMs which they felt could be accurately delineated and treated using MRI/MRA without a DSA.

Potential future improvements of triple-MRA include the use of vessel selective acquisition for ASL-MRA which could improve nidus visualisation by avoiding issues with vessel superposition on MIP and further improve characterisation of feeding patterns (Lindner et al.,

2015, Golay et al., 2005). The improved spatial resolution of HD-TOF in our study was achieved through a compromise between coverage and acquisition time and to this end FOV was reduced to 50 mm in the cranio-caudal direction (table 1). This may require altering for planning of large AVMs that are not fully covered by this tight FOV, with a consequent increase in acquisition time. ASL-MRA is also a very flexible technique which enabled us to personalise image acquisition based on the individual characteristics of each patient. This is a well-recognised concept in DSA where different frame rates (3 to 7 time points/sec) are used depending on the filling velocity of the abnormality. To our knowledge, this is the first time that individualised timing of a dynamic MRA acquisition is used to scan brain AVMs (figure 2) and this concept should be further developed in future stages of triple-MRA implementation. In our study the arrival of contrast agent was not detected by CE-MRA in one patient due to accidental mistiming of the manual contrast agent injection with respect to the dynamic acquisition. This could be improved by the use of an automatic injection pump. We also relied on commercial software for all co-registration stages. Estimates of error have been provided by the manufactures for clinical use, however independent quantification of accuracy of co-registration can help establish how much of the observed discrepancy between triple-MRA and DSA volumes is caused by image processing factors. Finally, the use of triple-MRA as an alternative to DSA for AVM radiosurgery planning relies on the development of tools and software capable of integrating multimodality 4D data into the planning procedure. This is still to be fully accomplished and currently available software could be greatly improved by implementing co-registration of dynamic (4D) sequences and by enabling the visualisation of delineated targets on 4D datasets such as CE-MRA and ASL-MRA.

Conclusions

The technical feasibility of using triple-MRA for visualisation and delineation of brain AVMs for GKR planning has been demonstrated. Tighter and more precise delineation of AVM target volumes could be achieved by using triple-MRA for AVMs radiosurgery targeting. However, further research is required to ascertain the impact this may have in obliteration rates and ARE.

Declaration of interests: Ian Paddick performs ad-hoc consultancy work for Elekta AB, Sweden. Alvaro Rojas-Villabona held a three-year academic position funded by Elekta (UK) Limited. The remaining authors report no conflict of interest concerning the materials or methods used in this study or the findings specified in this paper.

References

Al-Shahi, R., Pal, N., Lewis, S. C., Bhattacharya, J. J., Sellar, R. J., Warlow, C. P. and Group, A. O. A. S. (2002) 'Observer agreement in the angiographic assessment of arteriovenous malformations of the brain', *Stroke,* 33(6), pp. 1501-8.

Amponsah, K., Ellis, T. L., Chan, M. D., Lovato, J. F., Bourland, J. D., deGuzman, A. F., Ekstrand, K. E., Munley, M. T., McMullen, K. P., Shaw, E. G. and Tatter, S. B. (2012) 'Retrospective analysis of imaging techniques for treatment planning and monitoring of obliteration for gamma knife treatment of cerebral arteriovenous malformation', *Neurosurgery,* 71(4), pp. 893-9.

Bednarz, G., Downes, B., Werner-Wasik, M. and Rosenwasser, R. H. (2000) 'Combining stereotactic angiography and 3D time-of-flight magnetic resonance angiography in treatment planning for arteriovenous malformation radiosurgery', *Int J Radiat Oncol Biol Phys,* 46(5), pp. 1149-54.

Bendszus, M., Koltzenburg, M., Burger, R., Warmuth-Metz, M., Hofmann, E. and Solymosi, L. (1999) 'Silent embolism in diagnostic cerebral angiography and neurointerventional procedures: a prospective study', *Lancet,* 354(9190), pp. 1594-7.

Brainlab 2011. Clinical White Paper: iPLAN automatic image fusion.

Brainlab 2017. White paper: cranial distortion correction.

Buis, D. R., Lagerwaard, F. J., Barkhof, F., Dirven, C. M., Lycklama, G. J., Meijer, O. W., van den Berg, R., Langendijk, H. A., Slotman, B. J. and Vandertop, W. P. (2005) 'Stereotactic radiosurgery for brain AVMs: role of interobserver variation in target definition on digital subtraction angiography', *Int J Radiat Oncol Biol Phys,* 62(1), pp. 246-52.

Buis, D. R., Lagerwaard, F. J., Dirven, C. M., Barkhof, F., Knol, D. L., van den Berg, R., Slotman, B. J. and Vandertop, W. P. (2007) 'Delineation of brain AVMs on MR-Angiography for the purpose of stereotactic radiosurgery', *Int J Radiat Oncol Biol Phys,* 67(1), pp. 308-16.

Cohen-Inbar, O., Lee, C. C., Xu, Z., Schlesinger, D. and Sheehan, J. P. (2015) 'A quantitative analysis of adverse radiation effects following Gamma Knife radiosurgery for arteriovenous malformations', *J Neurosurg,* 123(4), pp. 945-53.

Dawkins, A. A., Evans, A. L., Wattam, J., Romanowski, C. A., Connolly, D. J., Hodgson, T. J. and Coley, S. C. (2007) 'Complications of cerebral angiography: a prospective analysis of 2,924 consecutive procedures', *Neuroradiology,* 49(9), pp. 753-9.

Fifi, J. T., Meyers, P. M., Lavine, S. D., Cox, V., Silverberg, L., Mangla, S. and Pile-Spellman, J. (2009) 'Complications of modern diagnostic cerebral angiography in an academic medical center', *J Vasc Interv Radiol,* 20(4), pp. 442-7.

Golay, X., Petersen, E. T. and Hui, F. (2005) 'Pulsed star labeling of arterial regions (PULSAR): a robust regional perfusion technique for high field imaging', *Magn Reson Med,* 53(1), pp. 15-21.

Hamm, K. D., Klisch, J., Surber, G., Kleinert, G., Eger, C. and Aschenbach, R. (2008) 'Special aspects of diagnostic imaging for radiosurgery of arteriovenous malformations', *Neurosurgery,* 62(5 Suppl), pp. A44-52; discussion A52.

Jaccard, P. (1912) 'The distribution of the flora in the alpine zone.', *New Phytologist,* 11(2), pp. 37-50.

Kang, J., Huang, J., Gailloud, P., Rigamonti, D., Lim, M., Bernard, V., Ehtiati, T. and Ford, E. C. (2014) 'Planning evaluation of C-arm cone beam CT angiography for target delineation in stereotactic radiation surgery of brain arteriovenous malformations', *Int J Radiat Oncol Biol Phys,* 90(2), pp. 430-7.

Kano, H., Flickinger, J. C., Tonetti, D., Hsu, A., Yang, H. C., Flannery, T. J., Niranjan, A. and Lunsford, L. D. (2017) 'Estimating the Risks of Adverse Radiation Effects After Gamma Knife Radiosurgery for Arteriovenous Malformations', *Stroke,* 48(1), pp. 84-90.

Kano, H., Kondziolka, D., Flickinger, J. C., Yang, H. C., Flannery, T. J., Awan, N. R., Niranjan, A., Novotny, J., Jr. and Lunsford, L. D. (2012) 'Stereotactic radiosurgery for arteriovenous malformations, Part 3: outcome predictors and risks after repeat radiosurgery', *J Neurosurg,* 116(1), pp. 21-32.

Kaufmann, T. J., Huston, J., 3rd, Mandrekar, J. N., Schleck, C. D., Thielen, K. R. and Kallmes, D. F. (2007) 'Complications of diagnostic cerebral angiography: evaluation of 19,826 consecutive patients', *Radiology,* 243(3), pp. 812-9.

Kemeny, A. A., Dias, P. S. and Forster, D. M. (1989) 'Results of stereotactic radiosurgery of arteriovenous malformations: an analysis of 52 cases', *J Neurol Neurosurg Psychiatry,* 52(5), pp. 554-8.

Koltz, M. T., Polifka, A. J., Saltos, A., Slawson, R. G., Kwok, Y., Aldrich, E. F. and Simard, J. M. (2013) 'Long-term outcome of Gamma Knife stereotactic radiosurgery for arteriovenous malformations graded by the Spetzler-Martin classification', *J Neurosurg,* 118(1), pp. 74-83.

Leffers, A. M. and Wagner, A. (2000) 'Neurologic complications of cerebral angiography. A retrospective study of complication rate and patient risk factors', *Acta Radiol,* 41(3), pp. 204-10.

Leksell, L. (1983) 'Stereotactic radiosurgery', *J Neurol Neurosurg Psychiatry,* 46(9), pp. 797-803.

Levrier, O., Manera, L., Regis, J., Farnarier, P., Ruefenacht, D. and Raybaut, C. (2001) 'Advances in the contributions of imaging to stereotaxic localization of cerebral arteriovenous malformations for radiosurgery.', *Neurochirurgie,* 47(2-3 Pt 2), pp. 201-11.

Lindner, T., Jensen-Kondering, U., van Osch, M. J., Jansen, O. and Helle, M. (2015) '3D time-resolved vessel-selective angiography based on pseudo-continuous arterial spin labeling', *Magn Reson Imaging,* 33(6), pp. 840-6.

Lunsford, L. D., Kondziolka, D., Flickinger, J. C., Bissonette, D. J., Jungreis, C. A., Maitz, A. H., Horton, J. A. and Coffey, R. J. (1991) 'Stereotactic radiosurgery for arteriovenous malformations of the brain', *J Neurosurg,* 75(4), pp. 512-24.

Nagaraja, S., Capener, D., Coley, S. C., Lee, K. J., Wilkinson, I. D., Kemeny, A. A. and Griffiths, P. D. (2005) 'Brain arteriovenous malformations: measurement of nidal volume using a combination of static and dynamic magnetic resonance angiography techniques', *Neuroradiology,* 47(5), pp. 387-92.

Pollock, B. E., Storlie, C. B., Link, M. J., Stafford, S. L., Garces, Y. I. and Foote, R. L. (2017) 'Comparative analysis of arteriovenous malformation grading scales in predicting outcomes after stereotactic radiosurgery', *J Neurosurg,* 126(3), pp. 852-858.

Rojas-Villabona, A., Miszkiel, K., Kitchen, N., Jäger, R. and Paddick, I. (2016) 'Evaluation of the stability of the stereotactic Leksell Frame G in Gamma Knife radiosurgery', *J Appl Clin Med Phys,* 17(3), pp. 5944.

Safain, M. G., Rahal, J. P., Raval, A., Rivard, M. J., Mignano, J. E., Wu, J. K. and Malek, A. M. (2014) 'Use of cone-beam computed tomography angiography in planning for gamma knife radiosurgery for arteriovenous malformations: a case series and early report', *Neurosurgery,* 74(6), pp. 682-96.

Sandström, H. 2011. Variability in target delineation in stereotactic radiosurgery with Leksell Gamma Knife Perfexion and a perspective on radiobiological outcome: A multiobserver study. *Department of Medical Radiation Physics.* Stockholm: Stockholm University.

Seymour, Z. A., Sneed, P. K., Gupta, N., Lawton, M. T., Molinaro, A. M., Young, W., Dowd, C. F., Halbach, V. V., Higashida, R. T. and McDermott, M. W. (2016) 'Volume-staged radiosurgery for large arteriovenous malformations: an evolving paradigm', *J Neurosurg,* 124(1), pp. 163-74.

St George, E. J., Butler, P. and Plowman, P. N. (2002) 'Can magnetic resonance imaging alone accurately define the arteriovenous nidus for gamma knife radiosurgery?', *J Neurosurg,* 97(5 Suppl), pp. 464-70.

Starke, R. M., Kano, H., Ding, D., Lee, J. Y., Mathieu, D., Whitesell, J., Pierce, J. T., Huang, P. P., Kondziolka, D., Yen, C. P., Feliciano, C., Rodgriguez-Mercado, R., Almodovar, L., Pieper, D. R., Grills, I. S., Silva, D., Abbassy, M., Missios, S., Barnett, G. H., Lunsford, L. D. and Sheehan, J. P. (2017) 'Stereotactic radiosurgery for cerebral arteriovenous malformations: evaluation of long-term outcomes in a multicenter cohort', *J Neurosurg,* 126(1), pp. 36-44.

Suzuki, Y., Fujima, N., Ogino, T., Meakin, J. A., Suwa, A., Sugimori, H., Van Cauteren, M. and van Osch, M. J. (2017) 'Acceleration of ASL-based time-resolved MR angiography by acquisition of control and labeled images in the same shot (ACTRESS)', *Magn Reson Med*.

Taschner, C. A., Le Thuc, V., Reyns, N., Gieseke, J., Gauvrit, J. Y., Pruvo, J. P. and Leclerc, X. (2007) 'Gamma Knife surgery for arteriovenous malformations in the brain: integration of time-resolved contrast-enhanced magnetic resonance angiography into dosimetry planning. Technical note', *J Neurosurg,* 107(4), pp. 854-9.

van Beijnum, J., van der Worp, H. B., Buis, D. R., Al-Shahi Salman, R., Kappelle, L. J., Rinkel, G. J., van der Sprenkel, J. W., Vandertop, W. P., Algra, A. and Klijn, C. J. (2011) 'Treatment of brain arteriovenous malformations: a systematic review and meta-analysis', *JAMA,* 306(18), pp. 2011-9.

Willinek, W. A., Hadizadeh, D. R., von Falkenhausen, M., Urbach, H., Hoogeveen, R., Schild, H. H. and Gieseke, J. (2008) '4D time-resolved MR angiography with keyhole (4D-TRAK): more than 60 times accelerated MRA using a combination of CENTRA, keyhole, and SENSE at 3.0T', *J Magn Reson Imaging,* 27(6), pp. 1455-60.

Wrede, K. H., Johst, S., Dammann, P., Özkan, N., Mönninghoff, C., Kraemer, M., Maderwald, S., Ladd, M. E., Sure, U., Umutlu, L. and Schlamann, M. (2014) 'Improved cerebral time-of-flight magnetic resonance angiography at 7 Tesla--feasibility study and preliminary results using optimized venous saturation pulses', *PLoS One,* 9(9), pp. e106697.

Yen, C. P., Matsumoto, J. A., Wintermark, M., Schwyzer, L., Evans, A. J., Jensen, M. E., Shaffrey, M. E. and Sheehan, J. P. (2013) 'Radiation-induced imaging changes following Gamma Knife surgery for cerebral arteriovenous malformations', *J Neurosurg,* 118(1), pp. 63-73.

Yu, C., Petrovich, Z., Apuzzo, M. L., Zelman, V. and Giannotta, S. L. (2004) 'Study of magnetic resonance imaging-based arteriovenous malformation delineation without conventional angiography', *Neurosurgery,* 54(5), pp. 1104-; discussion 1108-10.

Al-Shahi, R., Pal, N., Lewis, S. C., Bhattacharya, J. J., Sellar, R. J., Warlow, C. P. and Group, A. O. A. S. (2002) 'Observer agreement in the angiographic assessment of arteriovenous malformations of the brain', *Stroke,* 33(6), pp. 1501-8.

Amponsah, K., Ellis, T. L., Chan, M. D., Lovato, J. F., Bourland, J. D., deGuzman, A. F., Ekstrand, K. E., Munley, M. T., McMullen, K. P., Shaw, E. G. and Tatter, S. B. (2012) 'Retrospective analysis of imaging techniques for treatment planning and monitoring of obliteration for gamma knife treatment of cerebral arteriovenous malformation', *Neurosurgery,* 71(4), pp. 893-9.

Bednarz, G., Downes, B., Werner-Wasik, M. and Rosenwasser, R. H. (2000) 'Combining stereotactic angiography and 3D time-of-flight magnetic resonance angiography in treatment planning for arteriovenous malformation radiosurgery', *Int J Radiat Oncol Biol Phys,* 46(5), pp. 1149-54.

Bendszus, M., Koltzenburg, M., Burger, R., Warmuth-Metz, M., Hofmann, E. and Solymosi, L. (1999) 'Silent embolism in diagnostic cerebral angiography and neurointerventional procedures: a prospective study', *Lancet,* 354(9190), pp. 1594-7.

Brainlab 2011. Clinical White Paper: iPLAN automatic image fusion.

Brainlab 2017. White paper: cranial distortion correction.

Buis, D. R., Lagerwaard, F. J., Barkhof, F., Dirven, C. M., Lycklama, G. J., Meijer, O. W., van den Berg, R., Langendijk, H. A., Slotman, B. J. and Vandertop, W. P. (2005) 'Stereotactic radiosurgery for brain AVMs: role of interobserver variation in target definition on digital subtraction angiography', *Int J Radiat Oncol Biol Phys,* 62(1), pp. 246-52.

Buis, D. R., Lagerwaard, F. J., Dirven, C. M., Barkhof, F., Knol, D. L., van den Berg, R., Slotman, B. J. and Vandertop, W. P. (2007) 'Delineation of brain AVMs on MR-Angiography for the purpose of stereotactic radiosurgery', *Int J Radiat Oncol Biol Phys,* 67(1), pp. 308-16.

Cohen-Inbar, O., Lee, C. C., Xu, Z., Schlesinger, D. and Sheehan, J. P. (2015) 'A quantitative analysis of adverse radiation effects following Gamma Knife radiosurgery for arteriovenous malformations', *J Neurosurg,* 123(4), pp. 945-53.

Colombo, F., Cavedon, C., Francescon, P., Casentini, L., Fornezza, U., Castellan, L., Causin, F. and Perini, S. (2003) 'Three-dimensional angiography for radiosurgical treatment planning for arteriovenous malformations', *J Neurosurg,* 98(3), pp. 536-43.

Dawkins, A. A., Evans, A. L., Wattam, J., Romanowski, C. A., Connolly, D. J., Hodgson, T. J. and Coley, S. C. (2007) 'Complications of cerebral angiography: a prospective analysis of 2,924 consecutive procedures', *Neuroradiology,* 49(9), pp. 753-9.

Fifi, J. T., Meyers, P. M., Lavine, S. D., Cox, V., Silverberg, L., Mangla, S. and Pile-Spellman, J. (2009) 'Complications of modern diagnostic cerebral angiography in an academic medical center', *J Vasc Interv Radiol,* 20(4), pp. 442-7.

Golay, X., Petersen, E. T. and Hui, F. (2005) 'Pulsed star labeling of arterial regions (PULSAR): a robust regional perfusion technique for high field imaging', *Magn Reson Med,* 53(1), pp. 15-21.

Hamm, K. D., Klisch, J., Surber, G., Kleinert, G., Eger, C. and Aschenbach, R. (2008) 'Special aspects of diagnostic imaging for radiosurgery of arteriovenous malformations', *Neurosurgery,* 62(5 Suppl), pp. A44-52; discussion A52.

Huang, Y. J., Hsu, S. W., Lee, T. F., Ho, J. T. and Chen, W. F. (2017) 'Consistency between Targets Delineated by Angiography, Computed Tomography, and Magnetic Resonance Imaging in Stereotactic Radiosurgery for Arteriovenous Malformation', *Stereotact Funct Neurosurg,* 95(4), pp. 236-242.

Jaccard, P. (1912) 'The distribution of the flora in the alpine zone.', *New Phytologist,* 11(2), pp. 37-50.

Kang, J., Huang, J., Gailloud, P., Rigamonti, D., Lim, M., Bernard, V., Ehtiati, T. and Ford, E. C. (2014) 'Planning evaluation of C-arm cone beam CT angiography for target delineation in stereotactic radiation surgery of brain arteriovenous malformations', *Int J Radiat Oncol Biol Phys,* 90(2), pp. 430-7.

Kano, H., Flickinger, J. C., Tonetti, D., Hsu, A., Yang, H. C., Flannery, T. J., Niranjan, A. and Lunsford, L. D. (2017) 'Estimating the Risks of Adverse Radiation Effects After Gamma Knife Radiosurgery for Arteriovenous Malformations', *Stroke,* 48(1), pp. 84-90.

Kano, H., Kondziolka, D., Flickinger, J. C., Yang, H. C., Flannery, T. J., Awan, N. R., Niranjan, A., Novotny, J., Jr. and Lunsford, L. D. (2012) 'Stereotactic radiosurgery for arteriovenous malformations, Part 3: outcome predictors and risks after repeat radiosurgery', *J Neurosurg,* 116(1), pp. 21-32.

Kaufmann, T. J., Huston, J., 3rd, Mandrekar, J. N., Schleck, C. D., Thielen, K. R. and Kallmes, D. F. (2007) 'Complications of diagnostic cerebral angiography: evaluation of 19,826 consecutive patients', *Radiology,* 243(3), pp. 812-9.

Kemeny, A. A., Dias, P. S. and Forster, D. M. (1989) 'Results of stereotactic radiosurgery of arteriovenous malformations: an analysis of 52 cases', *J Neurol Neurosurg Psychiatry,* 52(5), pp. 554-8.

Koltz, M. T., Polifka, A. J., Saltos, A., Slawson, R. G., Kwok, Y., Aldrich, E. F. and Simard, J. M. (2013) 'Long-term outcome of Gamma Knife stereotactic radiosurgery for arteriovenous malformations graded by the Spetzler-Martin classification', *J Neurosurg,* 118(1), pp. 74-83.

Leffers, A. M. and Wagner, A. (2000) 'Neurologic complications of cerebral angiography. A retrospective study of complication rate and patient risk factors', *Acta Radiol,* 41(3), pp. 204-10.

Leksell, L. (1983) 'Stereotactic radiosurgery', *J Neurol Neurosurg Psychiatry,* 46(9), pp. 797-803.

Levrier, O., Manera, L., Regis, J., Farnarier, P., Ruefenacht, D. and Raybaut, C. (2001) 'Advances in the contributions of imaging to stereotaxic localization of cerebral arteriovenous malformations for radiosurgery.', *Neurochirurgie,* 47(2-3 Pt 2), pp. 201-11.

Lindner, T., Jensen-Kondering, U., van Osch, M. J., Jansen, O. and Helle, M. (2015) '3D time-resolved vessel-selective angiography based on pseudo-continuous arterial spin labeling', *Magn Reson Imaging,* 33(6), pp. 840-6.

Lunsford, L. D., Kondziolka, D., Flickinger, J. C., Bissonette, D. J., Jungreis, C. A., Maitz, A. H., Horton, J. A. and Coffey, R. J. (1991) 'Stereotactic radiosurgery for arteriovenous malformations of the brain', *J Neurosurg,* 75(4), pp. 512-24.

Nagaraja, S., Capener, D., Coley, S. C., Lee, K. J., Wilkinson, I. D., Kemeny, A. A. and Griffiths, P. D. (2005) 'Brain arteriovenous malformations: measurement of nidal volume using a combination of static and dynamic magnetic resonance angiography techniques', *Neuroradiology,* 47(5), pp. 387-92.

Pollock, B. E., Storlie, C. B., Link, M. J., Stafford, S. L., Garces, Y. I. and Foote, R. L. (2017) 'Comparative analysis of arteriovenous malformation grading scales in predicting outcomes after stereotactic radiosurgery', *J Neurosurg,* 126(3), pp. 852-858.

Rojas-Villabona, A., Miszkiel, K., Kitchen, N., Jäger, R. and Paddick, I. (2016) 'Evaluation of the stability of the stereotactic Leksell Frame G in Gamma Knife radiosurgery', *J Appl Clin Med Phys,* 17(3), pp. 5944.

Safain, M. G., Rahal, J. P., Raval, A., Rivard, M. J., Mignano, J. E., Wu, J. K. and Malek, A. M. (2014) 'Use of cone-beam computed tomography angiography in planning for gamma knife radiosurgery for arteriovenous malformations: a case series and early report', *Neurosurgery,* 74(6), pp. 682-96.

Sandström, H. 2011. Variability in target delineation in stereotactic radiosurgery with Leksell Gamma Knife Perfexion and a perspective on radiobiological outcome: A multiobserver study. *Department of Medical Radiation Physics.* Stockholm: Stockholm University.

Seymour, Z. A., Sneed, P. K., Gupta, N., Lawton, M. T., Molinaro, A. M., Young, W., Dowd, C. F., Halbach, V. V., Higashida, R. T. and McDermott, M. W. (2016) 'Volume-staged radiosurgery for large arteriovenous malformations: an evolving paradigm', *J Neurosurg,* 124(1), pp. 163-74.

St George, E. J., Butler, P. and Plowman, P. N. (2002) 'Can magnetic resonance imaging alone accurately define the arteriovenous nidus for gamma knife radiosurgery?', *J Neurosurg,* 97(5 Suppl), pp. 464-70.

Starke, R. M., Kano, H., Ding, D., Lee, J. Y., Mathieu, D., Whitesell, J., Pierce, J. T., Huang, P. P., Kondziolka, D., Yen, C. P., Feliciano, C., Rodgriguez-Mercado, R., Almodovar, L., Pieper, D. R., Grills, I. S., Silva, D., Abbassy, M., Missios, S., Barnett, G. H., Lunsford, L. D. and Sheehan, J. P. (2017) 'Stereotactic radiosurgery for cerebral arteriovenous malformations: evaluation of long-term outcomes in a multicenter cohort', *J Neurosurg,* 126(1), pp. 36-44.

Suzuki, Y., Fujima, N., Ogino, T., Meakin, J. A., Suwa, A., Sugimori, H., Van Cauteren, M. and van Osch, M. J. P. (2018) 'Acceleration of ASL-based time-resolved MR angiography by acquisition of control and labeled images in the same shot (ACTRESS)', *Magn Reson Med,* 79(1), pp. 224-233.

Taschner, C. A., Le Thuc, V., Reyns, N., Gieseke, J., Gauvrit, J. Y., Pruvo, J. P. and Leclerc, X. (2007) 'Gamma Knife surgery for arteriovenous malformations in the brain: integration of time-resolved contrast-enhanced magnetic resonance angiography into dosimetry planning. Technical note', *J Neurosurg,* 107(4), pp. 854-9.

van Beijnum, J., van der Worp, H. B., Buis, D. R., Al-Shahi Salman, R., Kappelle, L. J., Rinkel, G. J., van der Sprenkel, J. W., Vandertop, W. P., Algra, A. and Klijn, C. J. (2011) 'Treatment of brain arteriovenous malformations: a systematic review and meta-analysis', *JAMA,* 306(18), pp. 2011-9.

Willinek, W. A., Hadizadeh, D. R., von Falkenhausen, M., Urbach, H., Hoogeveen, R., Schild, H. H. and Gieseke, J. (2008) '4D time-resolved MR angiography with keyhole (4D-TRAK): more than 60 times accelerated MRA using a combination of CENTRA, keyhole, and SENSE at 3.0T', *J Magn Reson Imaging,* 27(6), pp. 1455-60.

Wrede, K. H., Johst, S., Dammann, P., Özkan, N., Mönninghoff, C., Kraemer, M., Maderwald, S., Ladd, M. E., Sure, U., Umutlu, L. and Schlamann, M. (2014) 'Improved cerebral time-of-flight magnetic resonance angiography at 7 Tesla--feasibility study and preliminary results using optimized venous saturation pulses', *PLoS One,* 9(9), pp. e106697.

Yen, C. P., Matsumoto, J. A., Wintermark, M., Schwyzer, L., Evans, A. J., Jensen, M. E., Shaffrey, M. E. and Sheehan, J. P. (2013) 'Radiation-induced imaging changes following Gamma Knife surgery for cerebral arteriovenous malformations', *J Neurosurg,* 118(1), pp. 63-73.

Yu, C., Petrovich, Z., Apuzzo, M. L., Zelman, V. and Giannotta, S. L. (2004) 'Study of magnetic resonance imaging-based arteriovenous malformation delineation without conventional angiography', *Neurosurgery,* 54(5), pp. 1104-; discussion 1108-10.

Table 1. Triple-MRA scanning parameters.

Parameter	ASL survey	ASL-MRA	CE-MRA	HD-TOF
MRA type	Dynamic survey	Dynamic	Dynamic	Single time point
Scan duration (mins:sec)	0:54	5:58 - 12:24	3:19	08:54
Contrast				
Scan mode	3D	3D	3D	3D
Acquisition	T1 TFEPI	T1 TFE	T1 FFE	T1 FFE
T_R (ms)	12	4.5	3	25
T_E (ms)	5	2.5	1.1	3.45
Flip Angle (°)	10	10	25	25
Resolution				
FOV (RL x AP x CC, mm)	210 x 210 x 10	210 x 210 x 90	150 x 210 x 210	250 x 250 x 50
Acquisition	transversal	transversal	Sagittal	transversal
Slabs	1	1	1	4
Acquisition matrix	172 x 167 x 8	172 x 172 x 70	50 x 248 x 248	832 x 568 x 50
Acquired voxel size (mm)	1.22 x1.26 x1.3	1.22 x 1.22 x 1.3	3 x 0.85 x 0.85	0.3 x 0.44 x 1
Reconstruction matrix	256 x 256	256 x 256	288 x 288	1936 x 1936
Rec voxel size (mm)	0.82 x 0.82 x 0.65	0.82 x 0.82 x 0.65	1.5 x 0.73 x 0.73	0.13 x 0.13 x 0.5
Number of slices	8	140	100	100
SENSE factor	2.5	2.5	4/2	2
Dynamic acquisition				
Dynamic imaging mode	TFEPI	TFE	CENTRA keyhole	-
Number of phases	8	3	24	-
Phase interval (temporal resolution)	200	200- 300 ms	608 ms	-
Label delay	200	200 – 800 ms	-	-
Contrast	-	-	Multihance 0.2ml/Kg	Post-contrast

Table 2. Demographic details and AVM characteristics of the study subjects.

Age mean (min-max)			38 y (18-62)
Female, n (%)			10 (66%)
AVM location, n		Frontal	3
		Parietal	2
		Occipital	4
		Temporal	3
		Basal ganglia	2
		Post fossa	1
Lateralisation, %		Right	53%
		Left	47%
Presentation, n (%)		Intracranial bleed	10 (66%)
		Seizures	2 (14%)
		Incidental	3 (20%)
SMS n: 14 one case excluded	**Size, %**	< 3 cm	71%
		3-6 cm	22%
		> 6 cm	7%
	Eloquence, %	Non-eloquent	35%
		Eloquent	65%
	Drainage, %	Superficial only	43%
		Deep	57%

Table 3. AVM target volumes obtained using the standard DSA method and triple-MRA. DI is the percentage of DSA volume included in triple-MRA volume. DnI is the percentage of triple-MRA volume not included in DSA volume. CcI is the ratio of the overlap to the union of the two volumes.

Case	DSA volume (ml)	Triple-MRA volume (ml)	Percentage difference (%)	DI (%)	DnI (%)	CcI
1	3.03	2.48	(-)18.3	76	7	0.72
2	8.73	7.21	(-)17.5	71	14	0.63
3	4.96	4.96	(-)0.05	79	20	0.65
4	0.56	0.51	(-)10.7	71	20	0.60
5	3.69	3.29	(-)10.4	71	20	0.60
6	5.87	5.14	(-)13.2	72	17	0.63
7	10.77	9.89	(-)8.2	78	15	0.69
8	1.32	1.07	(-)18.7	71	12	0.65
9	0.10	0.09	(-)8.1	65	30	0.51
10	2.10	2.27	7.3	80	26	0.62
11	0.23	0.21	(-)9.8	74	18	0.64
12	1.29	1.13	(-)12.7	71	19	0.61
13	4.20	4.00	(-)4.4	75	20	0.63
14	7.63	6.68	(-)12.4	76	13	0.69
Mean 95%CI	3.89 ml 1.95-5.82	3.49 ml 1.77-5.21	(-)9.8% (-)13.9 - (-)5.6	73.5% 71.2-76	18% 14-21	0.63 0.6-0.66
Median range	3.35 ml 0.1-10.77	2.88 ml 0.09-9.89	(-)10.5% (-)18.7 - 7.3	73% 65-80	18.4% 7-30	0.63 0.5-0.72

Figure 1. Patients flow diagram and image analysis framework used for target delineation with DSA and triple-MRA. DSA volume is the radiosurgical target drawn for delivery of GKR using 2D projections of DSA together with post-contrast T1, TOF and T2 weighted MRI.

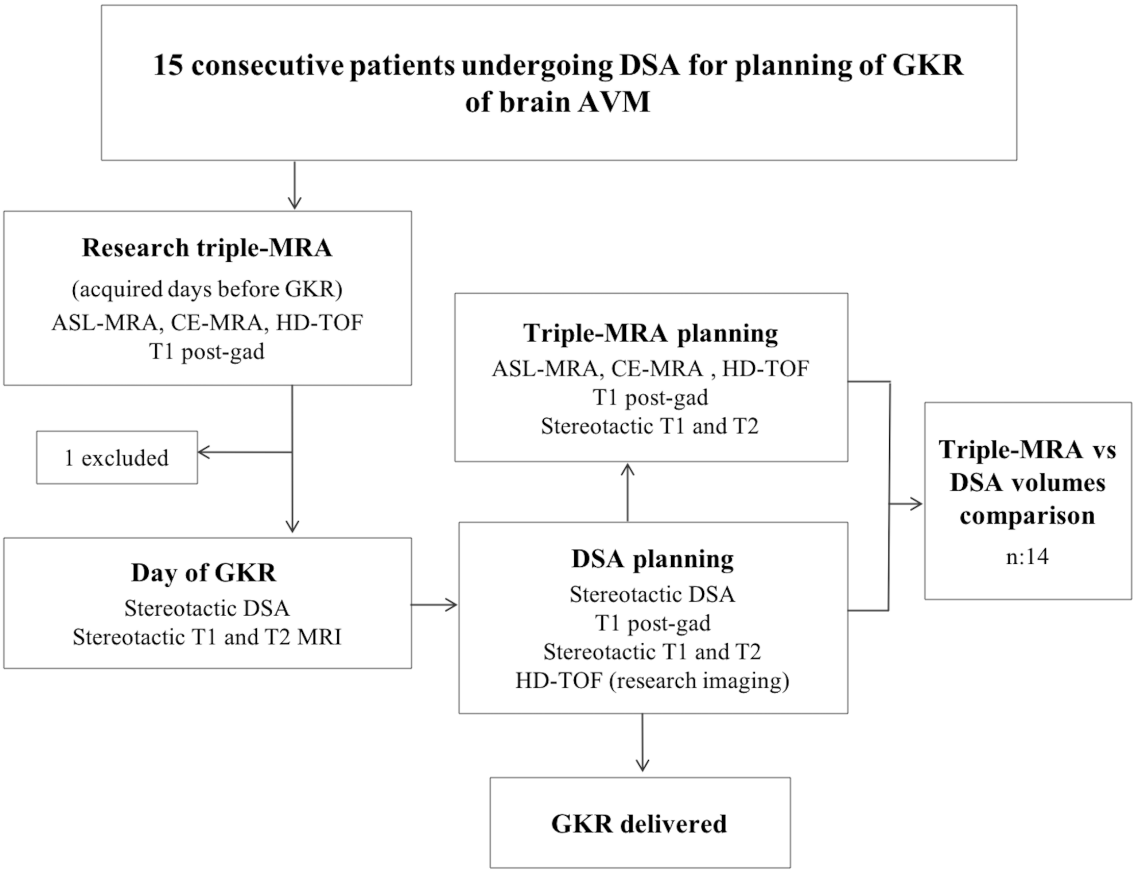

Figure 2. Representative example of the ASL survey developed to individualise timing of ASL-MRA. The ASL survey (left panel; temporal resolution: 200 ms; axial slab: 10 mm, acquisition time: 54 sec) enabled rapid characterisation of AVM filling velocity and the selection of three time points (500, 700 and 900 ms) in which the filling of the nidus is adequately visualised. The ASL-MRA acquisition is then limited to the selected time points (middle panel, AP MIP). The right panel shows the AP projection of DSA on the same patient for comparison.

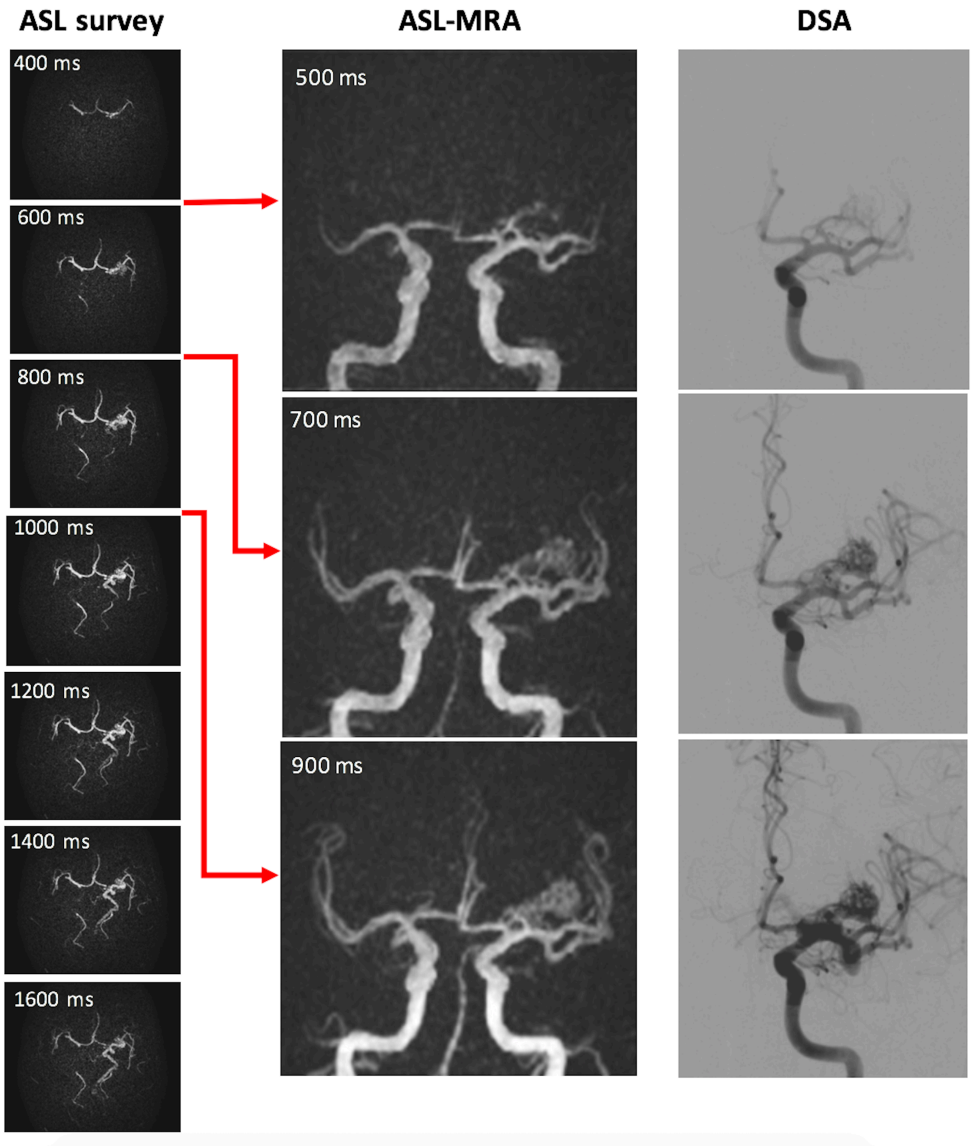

Figure 3. Imaging used for AVM delineation with the standard DSA based method and triple-MRA. Stereotactic DSA (D, E and F) together with standard volumetric MRI (top row A, B and C) is the current gold standard for AVM delineation. The limits (blue lines) of an AVM ROI delineated on 2D DSA images (blue contour) are projected into volumetric MRI defining an area within which the AVM is contained. A 3D volume is then drawn within this area on volumetric scans (DSA volume, orange). Triple-MRA volume, green ROI on volumetric MRI (G-H) is defined on co-registered HD-TOF (I), CE-MRA (J) and ASL MRA (K-L) as displayed on 360 degrees of freedom MIPs of all three MRA sequences (bottom row M, N and O).

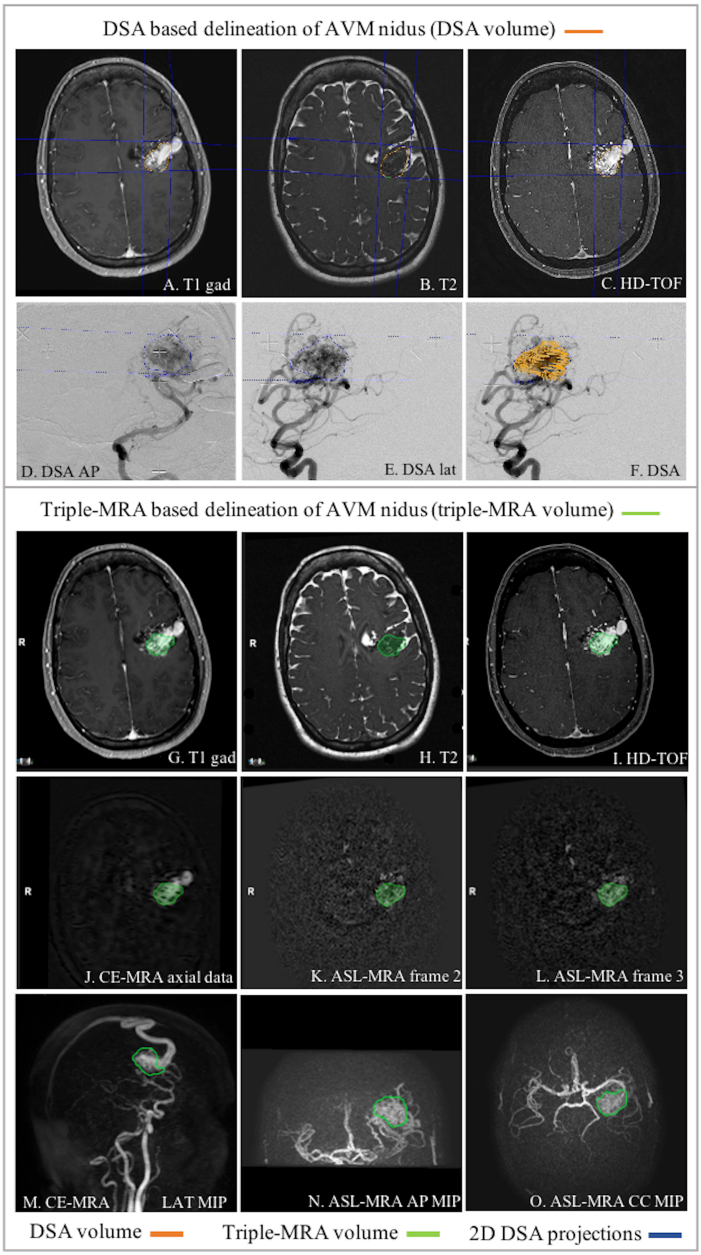

Figure 4. Bland-Altman plot of the difference between DSA and triple-MRA volumes.

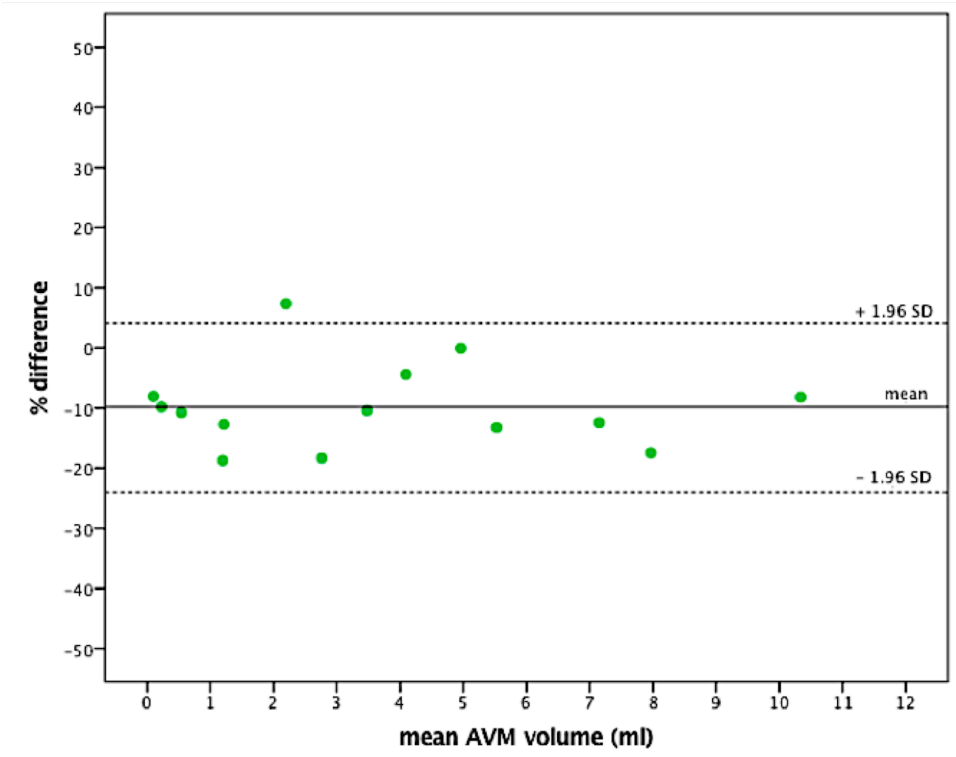

Figure 5. DSA and triple-MRA volumes in the case with the lowest DI and CcI. The DSA volume (orange) and triple-MRA volume (green) at five representative axial levels of the AVM in case 9 are shown on HD-TOF (column A) and post-gad T1 weighted MRI (column B). The two volumes are also displayed on the lateral and AP projections of DSA (columns C and D, respectively). During GKR planning the limits of the AVM ROI delineated on 2D DSA (blue contour) are projected into volumetric MRI scans to define an area within which the AVM is contained (blue projection lines).

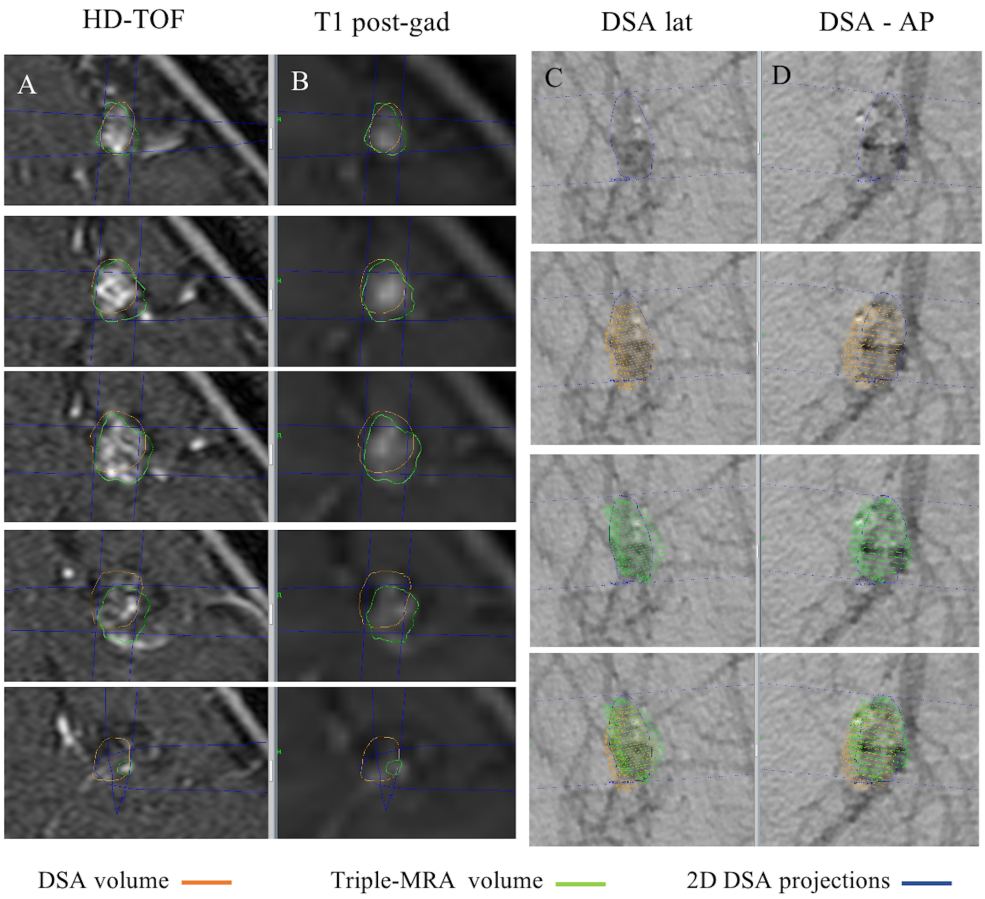

Figure 6. Case 10, in which triple-MRA volume was larger than DSA volume. The top two rows show two representative axial levels of the medial aspect of the AVM which appeared abnormal (red arrows) on HD-TOF (left) and T1 post-gad (right). This was consequently included on triple-MRA volume (green). Only very slight and diffuse vasculature is noted in this area on DSA (third row, lateral and AP projections as labelled) and this resulted on DSA volume (orange) being smaller than triple-MRA volume in this case. In the bottom row, triple-MRA volume is projected on MIPs of CE-MRA, ASL-MRA and DSA lateral and AP projections (from the left) for comparative purposes.